A COMPARISON BETWEEN TRANSIENT HEAT TRANSFER MEASUREMENTS USING TLC AND IR THERMOGRAPHY

Stefan Brack*, Rico Poser, Jens von Wolfersdorf
Institute of Aerospace Thermodynamics (ITLR) University of Stuttgart, Stuttgart, D-70569
*Stefan.Brack@itlr.uni-stuttgart.de

Abstract. Narrowband thermochromic liquid crystals (TLCs) and infrared thermography (IRT) are compared in the context of spatially resolved and transient heat transfer measurements. For accurate measurements the TLC coating was calibrated with a stationary method before the experiment. The IRT camera was in-situ calibrated with a surface thermocouple. A good agreement on temperature was achieved for both methods. The TLC data as a single-point-in-time measurement was evaluated for a time-independent heat transfer coefficient h_{TLC}. The surface temperature history measured with the IRT camera enables an additional evaluation for a time-dependent $h_{\mathrm{IR}}(t)$. In the case of one-dimensional heat conduction situations and late TLC indications, h_{TLC} and $h_{\mathrm{IR}}(t)$ agree well after the first $10\,\mathrm{s}$ of the experiment.

An investigation of the heat transfer in the wake region of a vortex generator illustrated the influence of lateral conduction. This effect is taken into account by an analytical-empirical correction method for the TLC data. For the IRT data an evaluation method based on an analytical solution of the three-dimensional heat conduction equation is presented. Equally to the one-dimensional case the evaluation methods considering the lateral conduction effects agree well after $10\,\mathrm{s}$ while the other methods deliver erroneous results.

Keywords: TLC, IR Thermography, Heat transfer, Lateral heat conduction

1 INTRODUCTION

The cooling development of modern heat exchangers, gas turbines and thermal equipment is still driven by experimental investigations of the heat transfer. As a result of the complex-shaped cooling geometries like for example skewed ribs, pin fins or swirl chambers, measurement techniques delivering distributions of the surface heat transfer coefficient are state of the art.

The heat transfer coefficient

$$h = \frac{\dot{q}_{\mathrm{S}}}{T_{\mathrm{ref}} - T_{\mathrm{S}}} \tag{1}$$

as a ratio of surface heat flux $\dot{q}_{\mathrm{S}}$ and driving temperature difference between the fluid reference temperature T_{ref} and the surface temperature T_{S} is only indirectly measurable. Therefore, it is often evaluated investigating the wall heat conduction with spatially resolved T_{S} measurements in combination with transient experiments.

The use of a thermochromic liquid crystal (TLC) coating is one widely spread possibility to measure T_{S}. Narrowband TLC with the indication band of about $1\,\mathrm{K}$ achieve accurate single-point-in-time temperature measurements at each position in a transient experiment but result in necessary assumptions for the evaluation method (Ireland and Jones, 2000). A main assumption is a time-independent h. Wideband TLC indicate over a broader temperature range but suffer from the increasing uncertainty for broader temperature bands (Newton *et al.*, 2003).

Another T_{S} measurement technique, also applicable to this type of experiments, is the infrared thermography (IRT) (Meola and Carlomagno, 2004; Bons, 2009; Bons *et al.*, 2009; Helmer, 2014). The recent advances in the IRT systems lead to systems with high accuracy, high spatial and temporal resolution (Helmer, 2014). The main advantages of the IRT systems compared to the TLC are the detection of the full T_{S} history, a broad temperature range and a relative insensitivity of the camera angle (Brauckmann and von Wolfersdorf, 2004). The main disadvantages are the necessity of an in-situ calibration for the measurement of absolute temperature levels, special optics with a high IR transmittance and the possible influence of the actual overall thermal situation.

In this study heat transfer measurement results evaluated with the aid of two different T_{S} measurement techniques are discussed. On the one hand T_{S} was measured with narrowband TLC and on the other hand an IRT camera delivered spatially resolved T_{S} distributions. For both types of T_{S} measurement data, evaluation techniques for 1D heat conduction cases as well as 3D heat conduction cases are presented. As both techniques measure simultaneously, the repeatability has no influence on the results.

The measurement data from the two T_{S} measurement methods is evaluated in different ways. For the TLC data the evaluation method is based on an analytical solution for a one-dimensional (1D) heat conduction process inside a semi-infinite wall with constant material properties (Metzger and Larson, 1986). In order to consider three-dimensional (3D) heat conduction effects an analytical-empirical correction method is applied as a post processing step (Brack *et al.*, 2016).

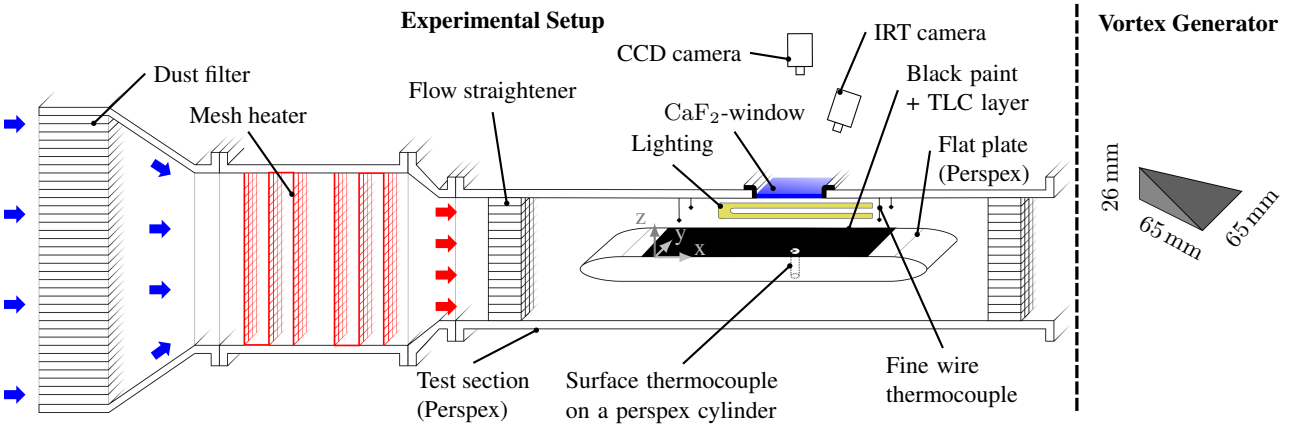

Figure 1: Experimental setup

The T_S histories received from the IRT camera are evaluated with the Cook-Felderman method derived by Cook and Felderman (1966) which delivers a time-dependent surface heat flux $\dot{q}_S\,(t)$. Equally to the analytical solution for the TLC data evaluation the Cook-Felderman method is valid for 1D heat conduction processes inside a semi-infinite wall with constant material properties. In contrast to the TLC data evaluation, three-dimensional conduction effects can be captured also with an analytical model described by Estorf (2006).

For comparison, two different heat transfer situations are evaluated. First the heat transfer on a flat plate and second the heat transfer in the wake region of a vortex generator.

2 EXPERIMENTAL SETUP

Figure 1 shows a schematic diagram of the experimental setup. During the experiment air from the ambient is sucked through the dust filter and heated up with the aid of a mesh heater. Six fine-wire meshes (three in series) connected to a power supply of $9.75\,\mathrm{kW}$ result in a sudden change of the fluid temperature and a homogeneous temperature distribution over the complete cross section. The perspex test section with a constant cross section of $120\,\mathrm{mm}$ times $150\,\mathrm{mm}$ follows directly downstream of the mesh heater.

The investigated heat transfer surface is part of a flat plate located in the symmetry plane of the test section. The test section as well as the flat plate are made of perspex (density $\rho = 1190\,{}^{\mathrm{kg}}/_{\mathrm{m}^3}$, specific heat capacity $c = 1470\,{}^{\mathrm{J}}/_{\mathrm{kgK}}$, thermal conductivity $k = 0.19\,{}^{\mathrm{W}}/_{\mathrm{mK}}$). In order to achieve acceptable measurement times complying the semi-infinite wall assumption, the thickness L of the flat plate is $30\,\mathrm{mm}$. Further the plate splits the test section into two sub-channels with a hydraulic diameter d_h of $80\,\mathrm{mm}$ each.

A $5\,\mathrm{mm}$ thick $\mathrm{CaF_2}$-window enclosed by an aluminum frame offers an optical access for the IRT camera as well as the CCD camera. With a transmittance above $95\,\%$ in the spectral range of both camera types, the $\mathrm{CaF_2}$-window ensures a strong measurement signal and low influence of the radiance of the surrounding.

Two fine-wire thermocouples in front and downstream the window measured the freestream temperature, applied as T_ref. A stationary calibration with a dry block calibrator (AMETEK$^{\mathrm{TM}}$ RCT-159B) reduced the uncertainty of the thermocouples to $0.2\,\mathrm{K}$. The wire diameter d_TC of the thermocouples is $0.08\,\mathrm{mm}$.

An NI-USB6218 data acquisition system combined with an I.E.D. thermocouple amplifier measured the voltages of the thermocouples at a sampling rate of $50\,\mathrm{Hz}$.

Above the test section a SONY DFW-X710 digital video camera with a frame rate of $15\,\mathrm{Hz}$ recorded the TLC color play uniformly illuminated by two $35\,\mathrm{W}$ warm white ($3000\,\mathrm{K}$) fluorescent lamps. For all experiments the surface of the flat plate was coated with two thin layers of black paint and TLC.

The calibration of the TLC indication temperature T_TLC delivered a value of $32.5\,^\circ\mathrm{C}$ (Hallcrest R31C1W, uncertainty $0.2\,\mathrm{K}$) for the maximum of the green color signal. Poser and von Wolfersdorf (2010) discuss the applied stationary calibration procedure in detail.

A FLIR SC7600 IRT camera at a frame rate of $25\,\mathrm{Hz}$ detected the surface radiation of the flat plate. The camera detector is sensitive in the spectral range from $1.5\,\mu\mathrm{m}$ to $5.1\,\mu\mathrm{m}$ and has a noise equivalent temperature difference value below $25\,\mathrm{mK}$. In order to in-situ calibrate the IRT camera, the flat plate includes one cylindrical sensor mount in the field of view. A $0.013\,\mathrm{mm}$ thick thin film surface thermocouple (OMEGA CO-2) glued on a perspex cylinder filled the sensor mount. Equally to the fine-wire thermocouples the thin film thermocouples were calibrated with the dry block calibrator.

With the vortex generator (VG) shown in Fig. 1 a variation of the investigated heat transfer pattern was realized. Mounting the VG on the top of the flat plate and in front of the $\mathrm{CaF_2}$-window leads to a locally strong varying heat transfer. The heat transfer variation is induced by the longitudinal vortex systems described by Henze *et al.* (2011).

3 DATA EVALUATION

The heat transfer coefficient h serves as the descriptive quantity of heat transfer in this study. It is deduced from the measured T_S evaluating the heat conduction inside the wall. Therefore the heat conduction equation

$$\frac{\partial T}{\partial t} = a\left[\frac{\partial^2 T}{\partial x^2} + \frac{\partial^2 T}{\partial y^2} + \frac{\partial^2 T}{\partial z^2}\right] \tag{2}$$

is solved. The given three-dimensional form implies constant material properties ρ, c, k of the wall which are combined to the thermal diffusivity $a = {}^{k}/_{\rho c}$.

Further for the given experimental setup the following initial condition

$$t = 0: \quad T = T_0\ , \tag{3}$$

representing a thermal equilibrium and the boundary condition

$$z = 0: \quad \frac{\partial T}{\partial z} = -\frac{h\,(t)}{k}\left[T\,(z=0,t) - T_\mathrm{ref}\,(t)\right] \tag{4}$$

are valid (coordinate system is shown in Fig. 1). The boundary condition delivers the connection between heat conduction and convective heat transfer. The negligible influence of the radiative heat transfer on the results is discussed in Section 3.2.

Depending on the applied T_S measurement technique further restrictions are necessary to receive an analytical solution of Eq. (2) discussed in the following subsections.

3.1 TLC DATA

One of the most widely spread transient TLC evaluation methods is based on a T_S change triggered by a sudden change in T_ref and starting at thermal equilibrium T_0. Recording the color change of the narrowband TLC delivers an accurate measurement of the time duration t_i for reaching

$$T_\mathrm{TLC} = T_\mathrm{S}|_{t=t_\mathrm{i}}\ . \tag{5}$$

With an additional measurement of the quantities T_0, $T_\mathrm{ref}\,(t)$ and an evaluation of the heat conduction inside the wall, a time-independent h_TLC can be calculated.

In the case of a 1D heat conduction situation Eq. (2) simplifies to

$$\frac{\partial T}{\partial t} = a\frac{\partial^2 T}{\partial z^2} \tag{6}$$

and can be solved analytically (Carslaw and Jaeger, 1959).

For an ideal step change in T_ref from T_0 to $T_{\mathrm{ref},\infty}$ and a semi-infinite wall one receives for the dimensionless surface temperature

$$\theta_\mathrm{S}^\mathrm{1D} = \frac{T_\mathrm{S} - T_0}{T_{\mathrm{ref},\infty} - T_0} = 1 - e^{\frac{\left[h_\mathrm{TLC}^\mathrm{1D}\right]^2 t}{\rho c k}}\,\mathrm{erfc}\left\{\frac{h_\mathrm{TLC}^\mathrm{1D}\sqrt{t}}{\sqrt{\rho c k}}\right\}\ . \tag{7}$$

As the ideal step change is experimentally difficult to achieve, $T_\mathrm{ref}\,(t)$ is often modeled with a series of step changes $\Delta T_{j,j-1}$ in $T_\mathrm{ref}\,(t)$ leading to the following evaluation equation

$$T_\mathrm{S} - T_0 = \sum_{j=1}^{N}\left[1 - e^{\frac{\left[h_\mathrm{TLC}^\mathrm{1D}\right]^2 (t-t_j)}{\rho c k}}\,\mathrm{erfc}\left\{\frac{h_\mathrm{TLC}^\mathrm{1D}\sqrt{t-t_j}}{\sqrt{\rho c k}}\right\}\right]\Delta T_{j,j-1}\ . \tag{8}$$

Besides Eq. (7) and Eq. (8), other analytical solutions for different experimental situations exist. Kwak (2008) discussed the modeling of the T_ref history with various functions like an exponential raise or an n-th order polynomial.

The semi-infinite wall assumption limits the duration t_d of the experiment. Schultz and Jones (1973) derived the criterion

$$t_\mathrm{d} < \frac{1}{16}\left[\frac{L}{2}\right]^2\frac{\rho c}{k} = 129.5\,\mathrm{s} \tag{9}$$

in order to ensure the compliance of the semi-infinite wall assumption for the given conditions.

The aforementioned evaluation equations are only valid for 1D heat conduction situations. Kingsley-Rowe *et al.* (2005) presented an analytical-empirical correction method to consider 2D heat conduction effects resulting from a spatial variation of h. Brack *et al.* (2016) expanded the approach to 3D heat conduction situations and an exponential T_{ref} change.

In order to simplify the 3D heat conduction equation but still capturing lateral conduction effects the lateral conduction ratio

$$\phi_{\mathrm{id}} = \frac{\partial^2 T/\partial x^2}{\partial^2 T/\partial z^2} + \frac{\partial^2 T/\partial y^2}{\partial^2 T/\partial z^2} \quad \rightarrow \quad \frac{\partial T}{\partial t} = a\frac{\partial^2 T}{\partial y^2}\left(1+\phi_{\mathrm{id}}\right) \tag{10}$$

is defined. Replacing ϕ_{id} with a constant average quantity $\overline{\phi_{\mathrm{id}}}$ leads to the 1D form of the heat conduction equation

$$\frac{\partial T}{\partial \bar{t}_{\mathrm{id}}} = a\frac{\partial^2 T}{\partial y^2}, \quad \bar{t}_{\mathrm{id}} = t\left(1+\overline{\phi_{\mathrm{id}}}\right) \ , \tag{11}$$

which is again analytically solvable. The correction quantity

$$\overline{\phi_{\mathrm{id}}} = c_{\mathrm{id}}^{3\mathrm{D}}\left[\left.\frac{\partial^2\theta_{\mathrm{S}}^{1\mathrm{D}}/\partial x^2}{\partial^2\theta_{\mathrm{S}}^{1\mathrm{D}}/\partial z^2}\right|_{t=t_i} + \left.\frac{\partial^2\theta_{\mathrm{S}}^{1\mathrm{D}}/\partial y^2}{\partial^2\theta_{\mathrm{S}}^{1\mathrm{D}}/\partial z^2}\right|_{t=t_i}\right] \tag{12}$$

consists of an empirical constant $c_{\mathrm{id}}^{3\mathrm{D}}$ and the conduction ratios. Both ratios are calculated with $\theta_{\mathrm{S}}^{1\mathrm{D}}$ (Eq. (7)) for the indication time t_{i} of the TLC. Several numerical simulations delivered correlations for the empirical constant $c_{\mathrm{id}}^{3\mathrm{D}}$ (Kingsley-Rowe *et al.*, 2005; Brack *et al.*, 2016).

Comparing the analytical solution for T_{S} received from Eq. (11) with Eq. (7) delivers an equation to calculate the corrected heat transfer coefficient

$$h_{\mathrm{TLC}}^{3\mathrm{D}} = \frac{h_{\mathrm{TLC}}^{1\mathrm{D}}}{\sqrt{1+\overline{\phi_{\mathrm{id}}}}} \ . \tag{13}$$

As the calculation of $h_{\mathrm{TLC}}^{3\mathrm{D}}$ includes the results received with the 1D heat conduction model, $h_{\mathrm{TLC}}^{3\mathrm{D}}$ is calculated in a post processing following the 1D evaluation. Equation (10) includes the analytical solution for T_{S} in the case of an ideal T_{ref} step change. The mathematical form of $\overline{\phi}$ in the case of an exponential T_{ref} change is discussed by Brack *et al.* (2016).

For the experimental results presented in this publication the TLC data is evaluated with Eq. (8) and in the case of 3D heat conduction situations $h_{\mathrm{TLC}}^{3\mathrm{D}}$ is calculated with $\overline{\phi_{\mathrm{id}}}$.

3.2 IRT DATA

Heat transfer evaluation While the TLC data evaluation methods include the necessity of a time-independent h, the measurement of the complete T_{S} history with the IRT camera offers the possibility to rearrange the boundary condition given in Eq. (4) to

$$z=0: \quad k\frac{\partial T}{\partial z} = \dot{q}_{\mathrm{S}}\left(t\right) \ . \tag{14}$$

Hence a direct calculation of the surface heat flux history ($\dot{q}_{\mathrm{S}}\left(t\right)$) is possible. Additionally $\dot{q}_{\mathrm{S}}\left(t\right)$ is independent from T_{ref} in contrast to the TLC evaluation methods.

For a 1D heat conduction situation within a semi-infinite wall and constant material properties, Schultz and Jones (1973) derived the analytical solution of the surface heat flux

$$\dot{q}_{\mathrm{S}}\left(t\right) = \sqrt{\frac{\rho c k}{\pi}}\left[\frac{T_{\mathrm{S}}\left(t\right)}{\sqrt{t}} + \frac{1}{2}\int_0^t \frac{T_{\mathrm{S}}\left(t\right)-T_{\mathrm{S}}\left(\tau\right)}{\left(t-\tau\right)^{3/2}}d\tau\right] \ . \tag{15}$$

With a piece-wise linear approximation of the T_{S} history

$$t_i < \tau < t_{i+1}: \quad T_{\mathrm{S}}\left(\tau\right) = \frac{T_{\mathrm{S}}\left(t_{i+1}\right)-T_{\mathrm{S}}\left(t_i\right)}{t_{i+1}-t_i}\left(\tau-t_i\right)+T_{\mathrm{S}}\left(t_i\right) \tag{16}$$

the integral in Eq. (15) is numerically solvable. The approximation results in a finite sum

$$\dot{q}_{\mathrm{S,CF}}\left(t\right) = \frac{2\sqrt{\rho c k}}{\sqrt{\pi}}\sum_{j=1}^{n}\frac{T_{\mathrm{S}}\left(t_j\right)-T_{\mathrm{S}}\left(t_{j-1}\right)}{\sqrt{t_n-t_j}-\sqrt{t_n-t_{j-1}}} \tag{17}$$

also known as the Cook-Felderman method.

Capturing spatial variations of h and T_{ref}, which induce lateral conduction effects, requires the application of a different evaluation method. Within the scope of this publication the evaluation method derived by Estorf (2006) is applied.

The analytical solution for an instantaneous area-related heat release of $2q_{\mathrm{S}}\left(x,y,z=0\right)$ in the xy-plane of infinite solid forms the basic equation of the method and is described with the initial condition

$$t=0: \quad \theta\left(x,y,z\right)=\frac{2q_{\mathrm{S}}\left(x,y\right)}{\rho c}\delta\left(z\right) \ . \tag{18}$$

The temperature is normalized with the initial temperature to $\theta=T-T_0$ and the Dirac-function $\delta\left(z\right)$ concentrates the energy to the xy-plane. As a consequence of the symmetry with respect to the xy-plane, the heat release splits up equally leading to a symmetrical heat flux field inside the infinite body for $t>0\,\mathrm{s}$.

A Fourier transformation in space simplifies the 3D heat conduction equation (Eq. (2)) to an ordinary differential equation

$$\frac{\partial\left[\tilde{\theta}\left(u,v,w,t\right)\right]}{\partial t}=-a\left(u^2+v^2+w^2\right)\tilde{\theta}\left(u,v,w,t\right) \ . \tag{19}$$

The quantities u, v and w represent the frequencies corresponding to x, y and z and $\tilde{\theta}$ the fourier transform of θ. The ordinary differential equation of Eq. (19) leads with the initial condition to the solution

$$\tilde{\theta}\left(u,v,w,t\right)=\frac{2}{\rho c}q_{\mathrm{S}}\left(u,v\right)\mathrm{e}^{-a\left(u^2+v^2+w^2\right)t} \ . \tag{20}$$

As q_{S} is not a function of the frequency w, an inverse transformation in z delivers

$$\tilde{\theta}\left(u,v,z,t\right)=\frac{1}{\rho c\sqrt{\pi a t}}q_{\mathrm{S}}\left(u,v\right)\mathrm{e}^{-a\left(u^2+v^2\right)t-\frac{z^2}{4at}} \ . \tag{21}$$

The boundary condition of the experimental setup is a time-dependent $\dot{q}_{\mathrm{S}}\left(x,y,z=0,t\right)$. With the aid of the Duhamel's principle, discussed in detail by Özişik (2013), Eq. (20) is modified to consider the time-dependent boundary condition leading to

$$\tilde{\theta}\left(u,v,z,t\right)=\frac{1}{\rho c\sqrt{\pi a}}\int_0^t\dot{q}_{\mathrm{S}}\left(u,v,\tau\right)\frac{\mathrm{e}^{-a\left(u^2+v^2\right)(t-\tau)-\frac{z^2}{4a(t-\tau)}}}{\sqrt{t-\tau}}\mathrm{d}\tau \ . \tag{22}$$

The mathematical steps to get the inverse of Eq. (22)

$$\dot{q}_{\mathrm{S}}\left(u,v,t\right)=\frac{k}{\sqrt{\pi a}}\int_0^t\frac{\partial\left(\tilde{\theta}\left(u,v,z=0,\tau\right)\mathrm{e}^{-a\left(u^2+v^2\right)(t-\tau)}\right)}{\partial\tau}\frac{1}{\sqrt{t-\tau}}\mathrm{d}\tau \tag{23}$$

are discussed in detail by Estorf (2006). Identically to the Cook-Felderman method a linear approximation of T_{S}, given in Eq. (16), results in a finite sum for the surface heat flux

$$\begin{aligned}\dot{q}_{\mathrm{S},lm}^{n}=k\sum_{k=0}^{n-1}\Bigg\{&\left[\left(\frac{1}{2\omega_{lm}a}+\omega_{lm}\left(t_n-t_k\right)\right)\frac{\tilde{\theta}_{lm,k+1}-\tilde{\theta}_{lm,k}}{\Delta t}+\omega_{lm}\tilde{\theta}_{lm,k}\right]\left(\mathrm{erf}\left[f_{lm}\left(t_k\right)\right]-\mathrm{erf}\left[f_{lm}\left(t_{k+1}\right)\right]\right)\\&+\frac{\tilde{\theta}_{lm,k+1}-\tilde{\theta}_{lm,k}}{\sqrt{\pi a}\Delta t}\left(\sqrt{t_n-t_k}\mathrm{e}^{-a\omega_{lm}^2(t_n-t_k)}-\sqrt{t_n-t_{k+1}}\mathrm{e}^{-a\omega_{lm}^2(t_n-t_{k+1})}\right)\Bigg\} \ .\end{aligned} \tag{24}$$

In addition a uniform discretization of the evaluated surface (L x M) leads to discrete frequencies u_l and v_m substituted with $\omega_{lm}=\sqrt{u_l^2+v_m^2}$ and the function $f_{lm}\left(\tau\right)=\omega_{lm}\sqrt{a\left(t_n-\tau\right)}$. For the results presented in Section 6 only a cosine transformation was applied on θ resulting in adiabatic boundaries of the field of view.

Independently of the chosen heat flux evaluation method, the heat transfer coefficient $h_{\mathrm{IR}}\left(t\right)$ is calculated in a post processing step with Eq. (1). The heat transfer coefficient $h_{\mathrm{IR}}^{\mathrm{1D}}$ is calculated with the Cook-Felderman method while $h_{\mathrm{IR}}^{\mathrm{3D}}$ represents values considering lateral conduction effects using the surface heat flux from Eq. (24).

Radiation balance In the previous derivations for the calculation of h, the radiative heat transfer $\dot{q}_{\sigma,\mathrm{S}}$ of the flat plate with the surroundings was neglected. Nevertheless, the area related emitted radiation $M_{\mathrm{S}}=\varepsilon_{\mathrm{S}}\sigma T_{\mathrm{S}}^4$ of the coated surface serves as the measurement quantity of the infrared camera in combination with the surface thermocouple to determine T_{S}. Setting up a radiation balance proves the assumption of a neglectable $\dot{q}_{\sigma,\mathrm{S}}$ and delivers the composition of the detected radiation of the IRT camera $\dot{q}_{\mathrm{Cam},i}$ in the sensitive wavelength interval $\Delta\lambda$.

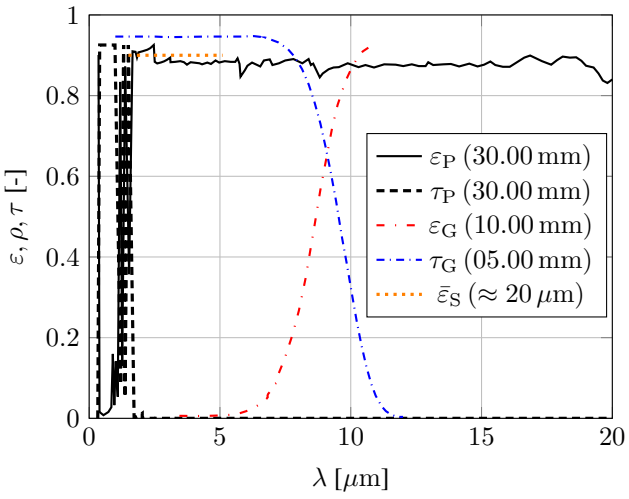

Figure 2: Wavelength-dependent emittance ε and transmittance τ of perspex (P) (Bal *et al.*, 2013), CaF_2 (G) (Rice, 1974) and the Black+TLC coating (S) for different material thicknesses

Table 1: Approximated wavelength-dependent properties of perspex, CaF_2 and the Black+TLC coating

Material	Property	Spectral range [μm] $\Delta\lambda_1$ 0-0.4	$\Delta\lambda_2$ 0.4-0.8	$\Delta\lambda_3$ 0.8-9.5	$\Delta\lambda_4$ 9.5-∞
Perspex	ε_P	0.91	0.03	$\|\leftarrow$	0.89
	ρ_P	0.09	0.05	$\|\leftarrow$	0.11
	τ_P	0.00	0.92	$\|\leftarrow$	0.00
CaF_2	ε_G	$\|\leftarrow$	0.00	$\rightarrow\|$	0.93
	ρ_G	$\|\leftarrow$	0.05	$\rightarrow\|$	0.07
	τ_G	$\|\leftarrow$	0.95	$\rightarrow\|$	0.00
Coating	ε_S	$\|\leftarrow$	0.90		$\rightarrow\|$
	ρ_S	$\|\leftarrow$	0.10		$\rightarrow\|$
	τ_S	$\|\leftarrow$	0.00		$\rightarrow\|$
$G(\Delta\lambda_i, 25\,^\circ\mathrm{C})$		≈ 0	≈ 0	23.52 %	76.48 %
$G(\Delta\lambda_i, 40\,^\circ\mathrm{C})$		≈ 0	≈ 0	26.70 %	73.30 %

The applicable method to set up a radiation balance for the experimental setup depends on the materials' wavelength-dependent radiation properties described by emittance ε, reflectance ρ and transmittance τ. For all materials, ε is regarded as diffuse. Therefore, hemispherical ε values were calculated with the available surface normal ε values and a conversion equation for dielectrics given by Howell *et al.* (2010). The conversion equation only depends on the refractive index n which reaches a value of 1.49 for perspex and 1.33 for CaF_2 (Bal *et al.*, 2013; Li, 1980). Furthermore, ρ can also be treated as diffuse as the experimental setup leads to multiple reflections (Siegel, 1973).

Figure 2 shows the wavelength-dependent hemispherical properties. For the black paint plus TLC coating no emittance properties were available. Therefore, the band emittance $\bar{\varepsilon}_S$ of the coating was measured with the IRT camera inside a climate chamber. Evaluating the measurements for different paint temperatures and ambient temperatures delivered a constant band emittance $\bar{\varepsilon}_S$ of 0.9.

Perspex as well as CaF_2 show sharp changes between high emittance and low transmittance and vice versa. In between the quantities are constant. A semigray approximation of the radiation properties, given in Tab. 1, enables the application of the net radiation method (Howell *et al.*, 2010). The area-related emitted heat flux splits up

$$M = \sum_{i=1}^{4} \underbrace{\varepsilon_i \sigma T^4}_{M^i} G(\Delta\lambda_i, T) \tag{25}$$

in a sum of M^i within the wavelength intervals $\Delta\lambda_i$ weighted with the fractional emission $G(\Delta\lambda_i, T)$ of a black body. Therefore, the radiation balance can be solved for every $\Delta\lambda_i$ independently.

Figure 3a shows the radiation balance inside the cross section of the experimental setup. Setting up the definition equation for each $\dot{q}_{o,k}$ leads to a solvable system of linear equations. Besides M_k^i, the outgoing radiation $\dot{q}_{o,k}^i$ includes the reflected radiation $\rho_k^i \dot{q}_{o,k}^i F_{k,l}$. The quantity $F_{k,l}$ represents the corresponding view factor between surface k and l. Walls in front and behind the CaF_2-window and the ambient are modeled as black body radiators. Consequently, the Stefan-Boltzmann law describes their radiation ($\dot{q}_{o,V} = \sigma T_V^4$, $\dot{q}_{o,H} = \sigma T_H^4$ and $M_{\infty,G} = \sigma T_\infty^4$) (Howell *et al.*, 2010).

The resulting radiative heat flux $\dot{q}_{\sigma,S}$ of the flat plate

$$\dot{q}_{\sigma,S} = \sum_{i=1}^{4} \left[\dot{q}_{o,S}^i - \dot{q}_{o,G}^i F_{S,G} - \dot{q}_{o,L}^i F_{S,L} - \dot{q}_{o,R}^i F_{S,R} - \dot{q}_{o,V}^i F_{S,V} - \dot{q}_{o,H}^i F_{S,H}\right] \tag{26}$$

is plotted in Fig. 3b for channel walls having all the same temperature ($T_S = T_L = T_R = T_G$). The linear approximation

$$\dot{q}_{\sigma,S} \approx \underbrace{\frac{\dot{q}_{\sigma,S}(T_S = 40\,^\circ\mathrm{C}) - \dot{q}_{\sigma,S}(T_S = T_\infty = 25\,^\circ\mathrm{C})}{15\,\mathrm{K}}}_{h_\sigma = 1.1\,\mathrm{W/m^2K}} (T_S - T_\infty) \tag{27}$$

delivers a comparable heat transfer coefficient h_σ to the convective h. The ambient temperature T_∞ reached for all experiments 25 °C and T_S never exceeded 40 °C. As the convective heat transfer coefficients are higher than $35\,\mathrm{W/m^2K}$ for all presented results, $\dot{q}_{\sigma,S}$ is not considered in the evaluation process.

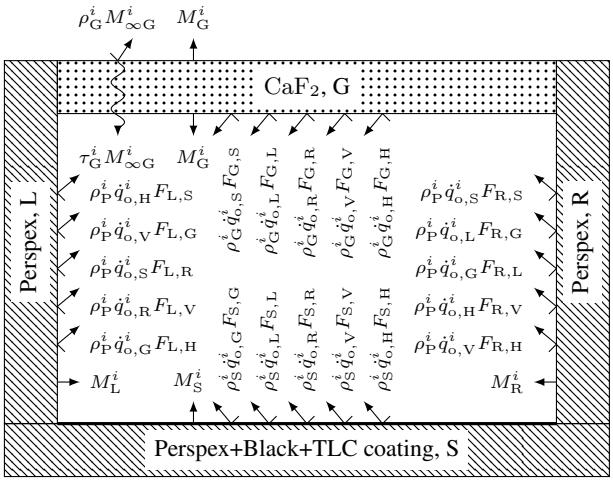

(a) Radiation balance

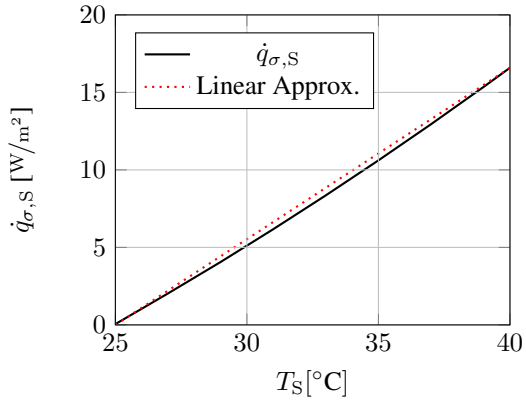

(b) Flat plate's radiative heat flux $\dot{q}_{\sigma,\mathrm{S}}$

Figure 3: Radiation balance for a wavelength interval $\Delta\lambda_i$ inside a cross section of the experimental setup and resulting flat plate radiative heat flux $\dot{q}_{\sigma,\mathrm{S}}$

The measured radiation of the IRT camera

$$\dot{q}_{i,\mathrm{Cam}} = F_{\mathrm{Cam,S}}\rho_{\mathrm{G}} M_{\infty,G} + F_{\mathrm{Cam,S}}\tau_G \dot{q}_{\mathrm{o,S}} \tag{28}$$

consists of the reflected ambient radiation $F_{\mathrm{Cam,S}}\rho_{\mathrm{G}} M_{\infty,G}$ and the transmitted outgoing radiation of the flat plate $F_{\mathrm{Cam,S}}\tau_G \dot{q}_{\mathrm{o,S}}$ in the wavelength interval of the camera. Approximating $G\,(1.5 - 5.1\,\mu\mathrm{m}, T)$ with an average temperature of $32.5\,^{\circ}\mathrm{C}$ for the radiation emitted by channel surfaces simplifies Eq. (28) to

$$\dot{q}_{i,\mathrm{Cam}} = \frac{F_{\mathrm{Cam,S}}}{56.98}\left[M_{\mathrm{S}} + 0.075 M_{\infty,G} + 0.016 M_{\mathrm{L}} + 0.016 M_{\mathrm{R}} + 0.011 M_{\mathrm{V}} + 0.011 M_{\mathrm{R}}\right] . \tag{29}$$

The mainly detected radiation is M_{S}. However, there is a constant influence of the ambient radiation $M_{\infty,G}$ and a varying influence of the radiation of the sidewalls of the channel. An in-situ calibration using the surface thermocouple offers the possibility to consider the influence of these additional radiation fluxes detected by the IRT camera.

4 Influence of TLC color change on IRT data

The goal of this study is the comparison of TLC and IRT heat transfer measurements. In order to get no influence of the repeatability of the experiments on the results, both techniques measured simultaneously the same heat transfer surface. However, it has to be ensured that both techniques do not influence each other while measuring.

The physical effect to measure temperature with TLCs is their change of the reflectance behavior in the visible spectrum with temperature. A possible influence in the IR range is investigated with a stationary experiment showing the complete play of colors of the TLC.

The experimental setup consists of a copper bar heated on the upper side and cooled on the lower side to realize a linear temperature gradient along the bar. Thermocouples directly underneath the surface of the bar measure the local temperature. One half of the surface is coated with black paint and TLC on the top. The other half is only coated with black paint. The graph in Fig. 4a includes a picture of the copper bar during the experiment. The graph to the right of the picture visualizes the temperature gradient measured with the thermocouples.

Besides the CCD camera also the IRT camera filmed the heated and coated copper bar. A contour plot of the IRT cameras $14\,\mathrm{bit}$ dimensionless output quantity DL is shown in Fig. 4b. As the TLC on top of the black paint change the emittance of the surface compared to black paint only, the spatial variation has to be considered. The band emittance $\bar{\varepsilon}$ of each region was determined by matching the temperatures received from the IRT measurement with the temperature measurements of the thermocouples.

Adjusting the emittance on each side leads to the same color gradient. As a consequence, the TLC change the surface emittance compared to the black coating but the color change of the TLC do not influence the detected radiation with the IRT camera. Consequently both measurement techniques do not influence each other during the experiment.

5 DATA COMPARISON

In order to compare the spatially resolved data received from the CCD camera and the IRT camera, a camera calibration for distortion was previously performed with LabVIEW VISION™. A printed calibration grid filmed with both cameras

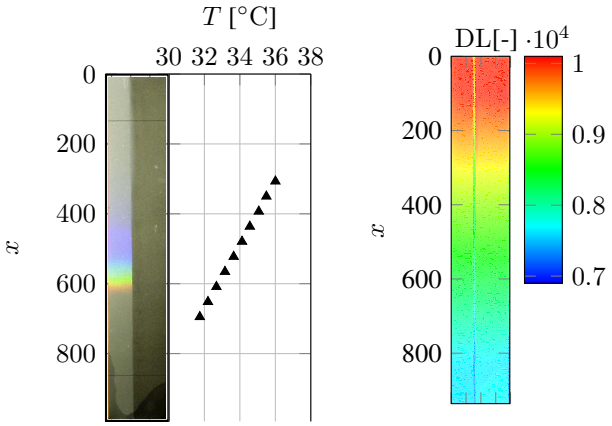

(a) CCD picture and coating temperature (b) Contour plot IRT picture

Figure 4: Influence of TLC color change on IRT-data

Table 2: Local comparison between TLC and IRT

Pos.	Exp.	t_i [s] TLC	t_i [s] IRT	$T_{S,IR} - T_{TLC}$ [K] for t_i^{TLC}
0	Slow	37.50	38.41	+0.07
	Fast	4.15	3.91	−0.25
1	Slow	47.90	45.65	−0.12
	Fast	5.27	4.70	−0.44
2	Slow	38.37	35.04	−0.24
	Fast	4.21	4.73	−0.50

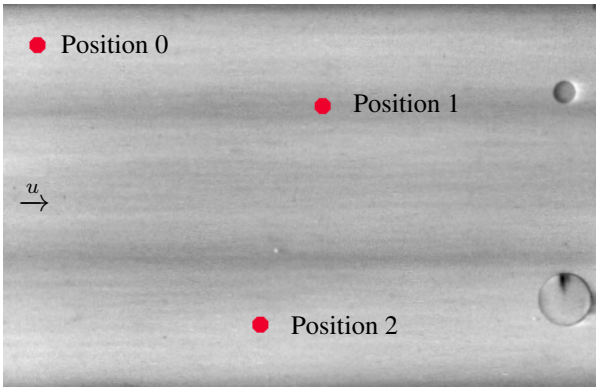

(a) Evaluation positions flat plate experiment

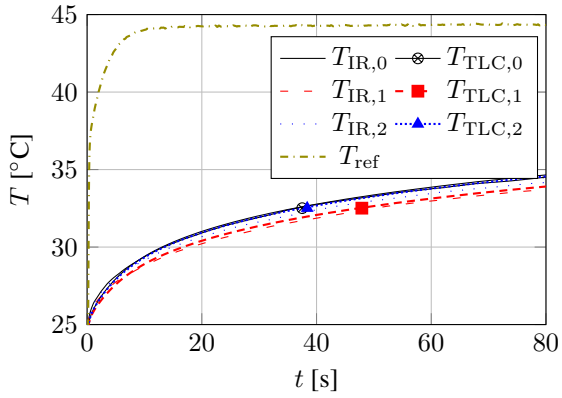

(b) Temperature histories and TLC indication for the slow flat plate experiment

Figure 5: Evaluation positions and temperature histories for the slow flat plate experiment

delivered the information to consider the distortion for every frame and to define a common coordinate system.

6 RESULTS

The following section presents the results of two different heat transfer situations evaluated with the TLC data as well as the IRT data. First a flat plate experiment with two different sudden fluid temperature changes illustrates the influence of the TLC indication time t_i. A small variation of T_ref ($\Delta T_\mathrm{ref} = T_{\mathrm{ref},\infty} - T_0 = 19\,\mathrm{K}$) leads to a relatively late TLC indication and a strong variation of T_ref ($\Delta T_\mathrm{ref} = 50\,\mathrm{K}$) leads to a relatively early TLC indication. The corresponding results are labeled with "Slow" and "Fast". The second part deals with the influence of lateral conduction on all discussed evaluation methods. Therefore, a VG was used to induce strong local variations in the heat transfer. All experiments were performed at the same sub-channel Re-number of $80,000$.

An uncertainty analysis according to Schulz *et al.* (2016) for h_TLC delivered a relative uncertainty of $10\ \%$ for all presented results (uncertainty of temperature measurements $0.2\,\mathrm{K}$, material properties $10\ \%$, timing $0.14\,\mathrm{s}$).

6.1 Indication time - Flat plate experiment

The grayscale picture in Fig. 5a illustrates the T_S distribution $10\,\mathrm{s}$ after the beginning of the experiment (dark - low temperatures, bright - high temperatures). The red dots mark the three local evaluation positions.

In Fig. 5b T_S is plotted against t for the evaluation points and the slow experiment. In addition to the measured T_S histories (IRT), the calculated T_S histories (TLC) are plotted. The calculated temperature histories were determined with Eq. (8) and the received h from the TLC data at indication time. Independent of measurement or calculation, all T_S histories show the same shape. However the absolute values deviate as t_i deviates. Thereby, t_i for the IRT measurements was determined as the time point where the IRT temperature equals the calibrated TLC temperature. Table 2 lists the

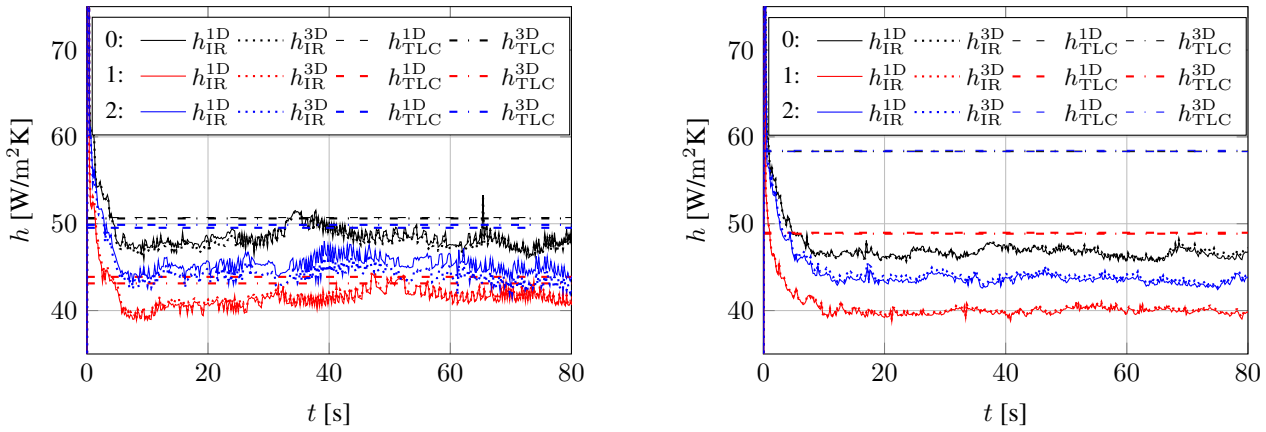

(a) Slow flat plate experiment

(b) Fast flat plate experiment

Figure 6: h histories for flat plate experiments

indication time t_i for the two experiments (slow and fast) and includes the temperature deviation $T_{\mathrm{S,IR}} - T_{\mathrm{TLC}}$ for t_i between the IRT data and the TLC data.

The slow experiment leads to large time lags between both T_S measurement techniques. The maximum deviation is 3.33 s for Position 1. But with respect to the temperature difference $T_{\mathrm{S,IR}} - T_{\mathrm{TLC}}$, these time lags are caused by the measurement uncertainties. As the gradient of T_S is low for late indications, also small differences between both measurement techniques lead to larger time lags. This fact is confirmed with the results of the fast experiment.

6.2 Heat transfer - Flat plate experiment

In Fig. 6a the determined heat transfer coefficients h of the slow experiment are plotted against t for the different evaluation methods. The time-independent h_{TLC} for the TLC method leads to constant values.

All evaluation methods show an approximately constant h in the same range for evaluation times greater than 10 s. Up to 10 s the results received from the TLC data differ from the IRT data results. While the TLC data heat transfer coefficients are time-independent per definition the IRT data heat transfer coefficients tend to high values for small evaluation times.

Comparing the heat transfer coefficients considering 1D heat conduction and 3D heat conduction for each T_S measurement technique shows that lateral conduction effects are negligible.

Figure 6b shows the h histories for the fast flat plate experiment. Again, lateral conduction effects still do not influence the evaluation results. But the deviation between h_{IR} and h_{TLC} is larger compared to the slow experiment.

The heat transfer coefficients h_{IR}, evaluated with the IRT data, are in a similar range and the history shows the same shape as for the slow flat plate experiment (see also Fig. 6a). However a larger difference between both experiments can be seen for h_{TLC}. All h_{TLC} values calculated with the data of the fast experiment are higher than in the case of the slow experiment. The results of TLC data evaluation methods as a single-point-in-time T_S measurement technique are dependent on the applied T_{ref} history. In comparison the $\dot{q}_\mathrm{S}$ history calculated with the IRT data only uses the T_S measurement.

6.3 Heat Transfer - Vortex generator experiment

Section 3 includes evaluation methods applicable to 1D heat conduction situations as well as evaluation methods for 3D heat conduction situations. Nevertheless, 1D methods are often preferred instead of 3D methods because of their lower computational effort. The following results give an impression of the influence of lateral conduction effects if 1D evaluation methods are used to evaluate 3D heat conduction situations.

Figure 7a shows the T_S distribution in the wake region of a vortex generator 10 s after the beginning of the experiment. The strong variation in T_S directly illustrates the variation in the heat transfer. In the downwash regions of the vortex systems T_S increases faster than in the upwash regions. As a result of the longitudinal vortex pairs one upwash region lies between two downwash regions and leads to strong lateral temperature gradients and lateral conduction effects.

A contour plot of the t_i-difference $\Delta t = t_\mathrm{i}^{\mathrm{IR}} - t_\mathrm{i}^{\mathrm{TLC}}$ between the TLC data and the IRT data is shown in Fig. 7b. Identically to the flat plate experiments late indication times lead to larger absolute values of Δt. Furthermore, the contours of the time differences are well related to the local h distribution. This indicates the different effects of the lateral conduction processes on the individual evaluation method.

Figure 8a presents the h histories for the three different evaluation points marked in Fig. 7a. Position 1, placed in the

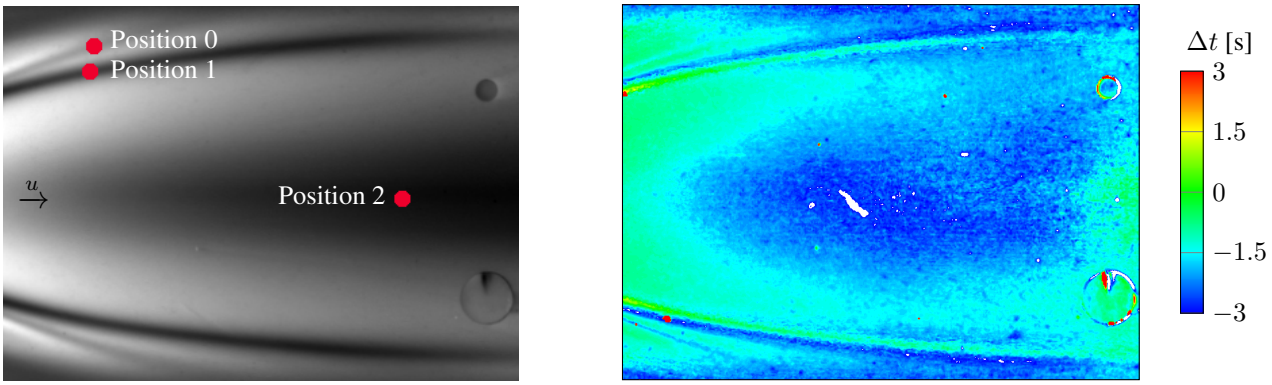

(a) Evaluation positions VG experiment

(b) Indication time difference Δt between IRT and TLC data

Figure 7: Evaluation positions and indication time difference for the VG experiment

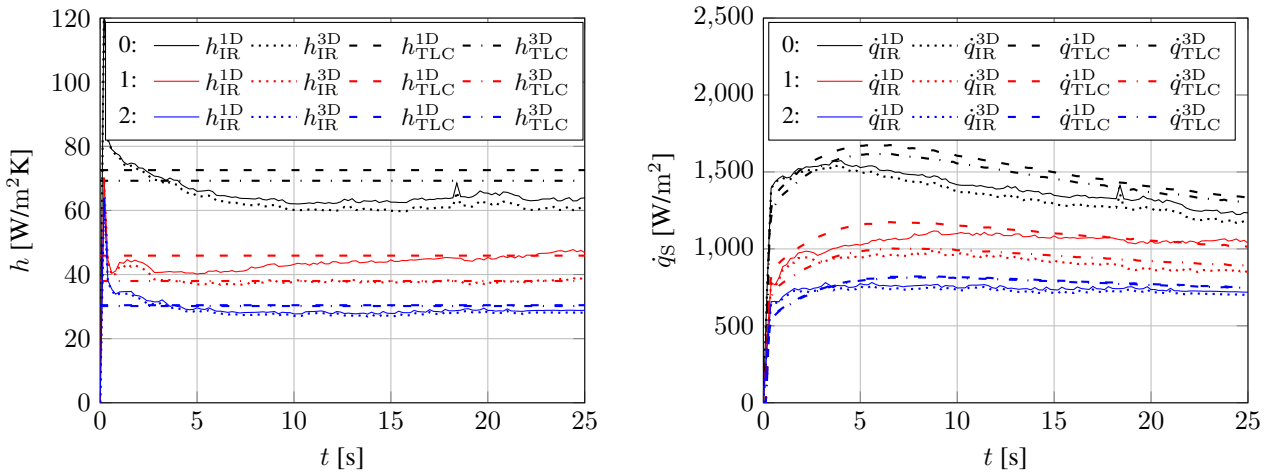

(a) h histories

(b) $\dot{q}_{\mathrm{S}}$ histories

Figure 8: Heat transfer characteristics of the VG-experiment for three different evaluation positions

upwash region of the longitudinal vortex pairs, experience strong lateral temperature gradients. The conductive lateral heat flux is continuously towards this position from the surrounding positions. Therefore $h_{\mathrm{TLC}}^{\mathrm{1D}}$ reaches a significantly higher value than $h_{\mathrm{TLC}}^{\mathrm{3D}}$. The heat transfer coefficient $h_{\mathrm{IR}}^{\mathrm{1D}}$ shows a continuous drift over time while $h_{\mathrm{IR}}^{\mathrm{3D}}$ is constant for evaluation times larger than 5 s. Further the values of $h_{\mathrm{TLC}}^{\mathrm{3D}}$ and $h_{\mathrm{IR}}^{\mathrm{3D}}$ agree.

For position 2, all calculated heat transfer coefficients agree. The local region around position 2 is slightly influenced by lateral conduction effects.

The largest difference between the heat transfer coefficients calculated with the different T_{S} measurement techniques can be seen for position 0. Nevertheless, the correction of lateral conduction for the TLC data as well the IRT data shows a decrease in h. An explanation for the difference between TLC data results and IRT data results is also the indication time t_i of the TLC. As noticed for the fast flat plate experiment in Section 6.2, faster indication times lead to higher heat transfer coefficients received with the TLC evaluation methods.

The graph in Fig. 8b shows the directly calculated $\dot{q}_{\mathrm{S,IR}}$-histories with the time-resolved IRT data on the one hand and the indirectly calculated $\dot{q}_{\mathrm{S,TLC}}$-histories of the TLC data on the other hand. In order to calculate $\dot{q}_{\mathrm{S,TLC}}$, a T_{S} history is calculated with the derived h_{TLC} and Eq. (8). Inserting the calculated T_{S} values with the corresponding T_{ref} values in Eq. (1) results in the time-resolved $\dot{q}_{\mathrm{TLC}}$ for the TLC data.

Independently of the evaluation methods the $\dot{q}_{\mathrm{S}}$ histories show the same shape. A sharp increase at the beginning up to the maximum value is followed by a slight decrease. For position 2 the results of all evaluation methods agree.

As a result of the strong lateral conduction effects at position 1, only the heat flux histories of the 3D methods agree. For the 1D methods the lateral heat fluxes are attributed to the surface normal heat flux $\dot{q}_{\mathrm{S}}$ leading in the case of the IRT data to an all along increasing $\dot{q}_{\mathrm{S}}^{\mathrm{IR}}$.

Identically to h evaluation results, the largest differences between the TLC data evaluation and the IRT data evaluation

is seen for position 0. The maximum value of $\dot{q}_\mathrm{S}$ as well as the point in time of the maximum differ.

7 CONCLUSIONS

Two surface temperature measurement techniques were compared and used for the data evaluation of transient heat transfer experiments. The investigated surface was coated with narrowband TLC. Additionally an IRT camera measured the radiation of the surface. As a result of the experimental setup, the IRT camera is not only influenced by the radiation of the investigated surface but also by the surrounding. A necessary in-situ calibration was performed with a surface thermocouple.

Both measurement techniques deliver the same surface temperatures in the range of the measurement uncertainties. Initially studies with low spatial variation of the heat transfer coefficient (flat plate) were performed. Then the heat transfer in the wake region of a vortex generator with a strong spatial variation of the heat transfer coefficient was investigated. The measurements of the narrowband TLC lead to time-independent heat transfer coefficients. The surface temperature histories of the IRT camera are used to calculate the surface heat flux histories and delivered time-dependent heat transfer coefficients.

The results of the flat plate experiments showed the importance of the TLC indication time. All evaluation methods agree well in the case of indication times approximately greater than $10\,\mathrm{s}$. An earlier indication or evaluation time leads to a larger deviation between the methods.

For the experiment with a vortex generator, larger deviations are detected depending on the evaluation position. Positions strongly influenced by lateral conduction show a time-dependent heat transfer coefficient for the $1\mathrm{D}$ IRT data evaluation method while the $3\mathrm{D}$ evaluation methods reaches again a constant value for evaluation times greater than $10\,\mathrm{s}$.

The analytical-empirical correction method for the TLC data and the $3\mathrm{D}$ evaluation method for the IRT data agree well except for position 0 in the vortex generator experiment. As a result of the early TLC indication time for position 0, the evaluated heat transfer coefficient is mainly influenced by the reference temperature history compared to lateral conduction effects. Concluding the comparison of both T_S measurement techniques and the corresponding evaluation methods showed their range of applicability and possible influencing factors on the evaluation results.

8 REFERENCES

Bal, N., Raynard, J., Rein, G., Torero, J., Försth, M., Boulet, P., Parent, G., Acem, Z. and Linteris, G., 2013. "Experimental study of radiative heat transfer in a translucent fuel sample exposed to different spectral sources". *International Journal of Heat and Mass Transfer*, Vol. 61, pp. 742–748.

Bons, J., 2009. "Transient method for convective heat transfer measurement with lateral conduction-Part I: Application to a deposit-roughened gas turbine surface". *Journal of Heat Transfer*, Vol. 131, No. 1.

Bons, J., Fletcher, D. and Borchert, B., 2009. "Transient method for convective heat transfer measurement with lateral conduction-Part II: Application to an isolated spherical roughness element". *Journal of Heat Transfer*, Vol. 131, No. 1.

Brack, S., Poser, R. and von Wolfersdorf, J., 2016. "An approach to consider lateral heat conduction effects in the evaluation process of transient heat transfer measurements using TLC". *International Journal of Thermal Sciences*, Vol. 107, pp. 289–302.

Brauckmann, D. and von Wolfersdorf, J., 2004. "Infrared thermography with in-situ calibration using thermochromic liquid crystals applied to film cooling". In *ASME Turbo Expo 2004: Power for Land, Sea, and Air*. American Society of Mechanical Engineers, pp. 779–785.

Carslaw, H.S. and Jaeger, J.C., 1959. *Conduction of Heat in Solids*. Oxford University Press, 2nd edition.

Cook, W. and Felderman, E., 1966. "Reduction of data from thin-film heat-transfer gages-a concise numerical technique." *AIAA journal*, Vol. 4, No. 3, pp. 561–562.

Estorf, M., 2006. "Image based heating rate calculation from thermographic data considering lateral heat conduction". *International journal of heat and mass transfer*, Vol. 49, No. 15, pp. 2545–2556.

Helmer, D.B., 2014. "Modified transient infrared methodology for leading edge impingement measurements". In *ASME Turbo Expo 2014: Turbine Technical Conference and Exposition*. American Society of Mechanical Engineers, pp. V05AT12A026–V05AT12A026.

Henze, M., Von Wolfersdorf, J., Weigand, B., Dietz, C. and Neumann, S., 2011. "Flow and heat transfer characteristics behind vortex generators–a benchmark dataset". *International Journal of Heat and Fluid Flow*, Vol. 32, No. 1, pp. 318–328.

Howell, J.R., Menguc, M.P. and Siegel, R., 2010. *Thermal radiation heat transfer*. CRC press.

Ireland, P. and Jones, T., 2000. "Liquid crystal measurements of heat transfer and surface shear stress". *Measurement Science and Technology*, Vol. 11, No. 7.

Kingsley-Rowe, J.R., Lock, G.D. and Owen, J.M., 2005. "Transient heat transfer measurements using thermochromic liquid crystal: lateral-conduction error". *International Journal of Heat and Fluid Flow*, Vol. 26, No. 2, pp. 256–263.

Kwak, J.S., 2008. "Comparison of analytical and superposition solutions of the transient liquid crystal technique". *Journal*

of Thermophysics and Heat Transfer, Vol. 22, No. 2, pp. 290–295.

Li, H., 1980. "Refractive index of alkaline earth halides and its wavelength and temperature derivatives". *Journal of Physical and Chemical Reference Data*, Vol. 9, No. 1, pp. 161–290.

Meola, C. and Carlomagno, G.M., 2004. "Recent advances in the use of infrared thermography". *Measurement science and technology*, Vol. 15, No. 9.

Metzger, D. and Larson, D., 1986. "Use of melting point surface coatings for local convection heat transfer measurements in rectangular channel flows with 90-deg turns". *Journal of Heat Transfer*, Vol. 108, No. 1, pp. 48–54.

Newton, P.J., Yan, Y., Stevens, N.E., Evatt, S.T., Lock, G.D. and Owen, J.M., 2003. "Transient heat transfer measurements using thermochromic liquid crystal. part 1: An improved technique". *International journal of heat and fluid flow*, Vol. 24, No. 1, pp. 14–22.

Özişik, M.N., 2013. *Boundary value problems of heat conduction*. Courier Corporation.

Poser, R. and von Wolfersdorf, J., 2010. "Transient liquid crystal thermography in complex internal cooling systems". *VKI LS 2010-05, Internal cooling in turbomachinery, ISBN 978-2-87516-006-5*.

Rice, R., 1974. "High energy laser windows". Technical report, DTIC Document.

Schultz, D.L. and Jones, T., 1973. "Heat-transfer measurements in short-duration hypersonic facilities." Technical report, DTIC Document AGARD-AG 165.

Schulz, S., Brack, S., Terzis, A., von Wolfersdorf, J. and Ott, P., 2016. "On the effects of coating thickness in transient heat transfer experiments using thermochromic liquid crystals". *Experimental Thermal and Fluid Science*, Vol. 70, pp. 196 – 207.

Siegel, R., 1973. "Net radiation method for enclosure systems involving partially transparent walls". Technical report, NASA TN D-7384.